

# Supporting Information

Wood et al. 10.1073/pnas.0915068107

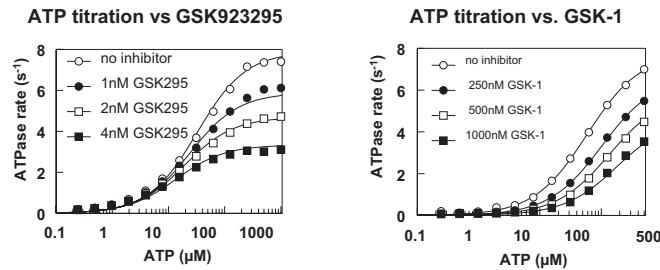


Fig. S1. Effect of ATP on inhibition of centromere-associated protein-E (CENP-E) MT-stimulated ATPase mode of inhibition studies of GSK923295 (Left) and GSK-1 (Right) varying ATP and inhibitor concentrations in the presence of saturating MT. The concentration of CENP-E motor domain in these reactions was 0.75 nM.

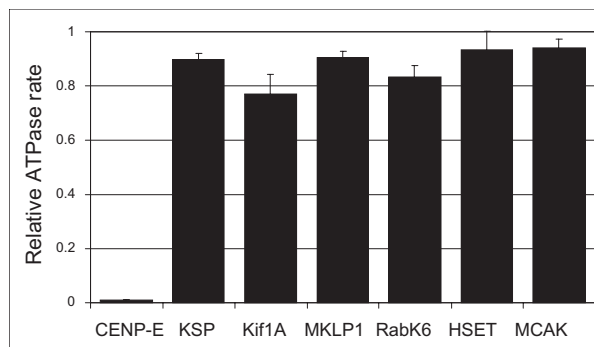


Fig. S2. Kinesin specificity of GSK923295 rates of microtubules (MT)-stimulated ATPase of multiple kinesin motor domains observed in the presence of 40 mM GSK923295. Rates are normalized to rates observed in the absence of inhibitor. Reactions were performed at substrate concentrations 5-fold the  $K_m$  of the respective kinesins for ATP and MT. Variation shown is standard deviation ( $n = 4$ ).

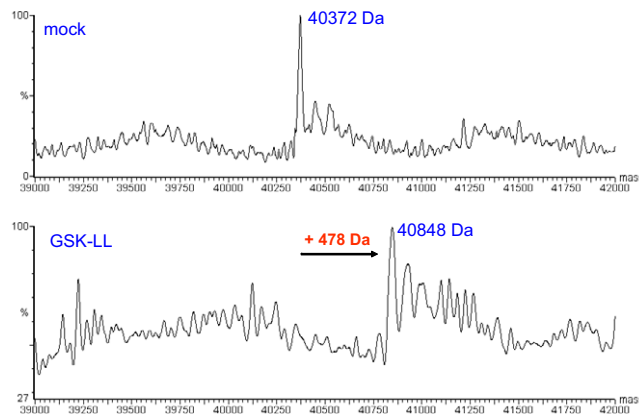
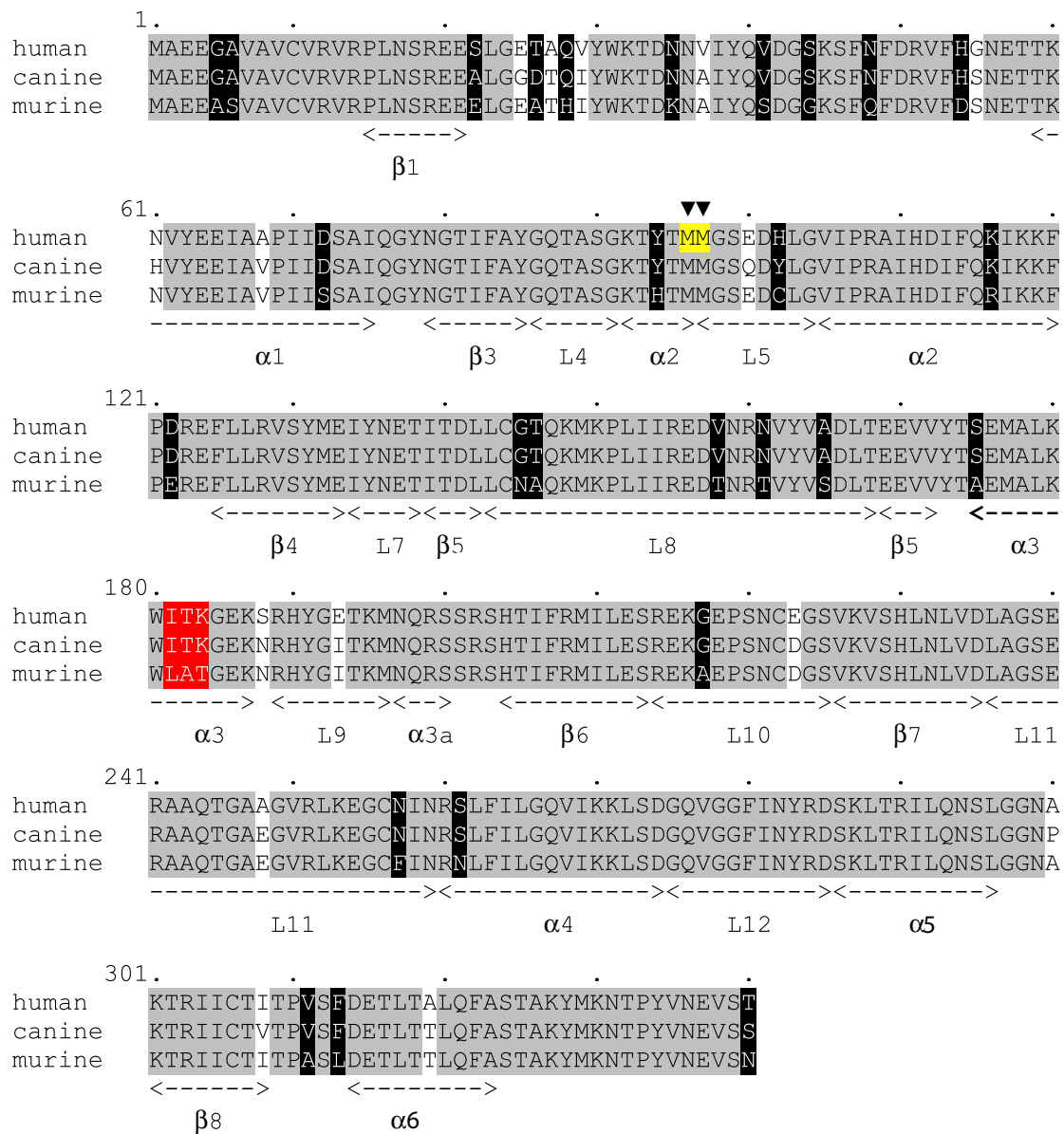
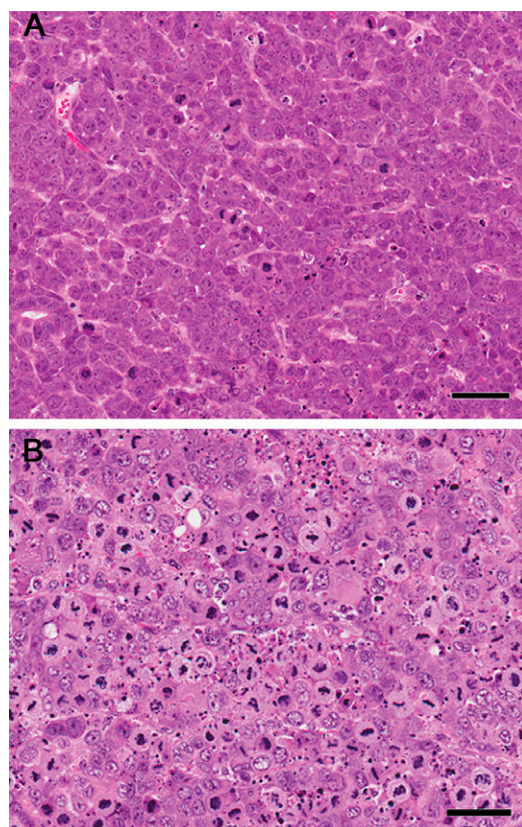


Fig. S3. Liquid chromatography-mass spectrometry analysis of 6His-tagged CENP-E motor domain photoaffinity labeled with GSK-1. Photo-affinity labeling with GSK-1 shows a quantitative shift in the mass of CENP-E motor domain of 478 Da, which corresponds to the mass of linked portion of GSK-1.

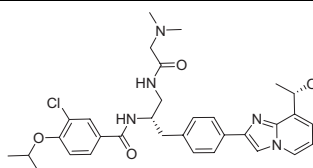
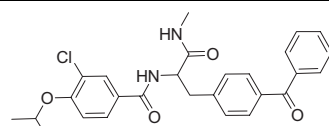
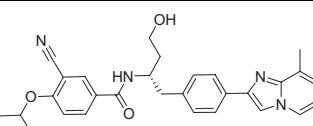


**Fig. 54.** Alignment of primary amino acid sequence of human, canine, and murine CENP-E motor domains. Residues identical in all three variant are indicated with gray shading. Residues where murine sequence is identical to either human or canine are unshaded, and residues in which murine sequence differs from both human and canine CENP-E are shaded black or red. Residues in human CENP-E photo-labeled with inhibitor GSK-2 (Table S1), Met96 and Met97, are shaded yellow and identified by arrowheads. Secondary structural features are annotated below the sequence, and the starting residue number of each line is noted on the left. Residues unique in murine CENP-E compared with either human or canine CENP-E are sparsely scattered across the motor domain. Residues Ile182, Thr183, and Lys184 in helix  $\alpha$ 3 evaluated in mutagenesis studies are highlighted in red shading.



**Fig. S5.** Tumor pharmacodynamic response to GSK923295. Representative photomicrographs of an H&E-stained section of Colo205 tumor xenografts removed from untreated mouse (A) or 24 h after a single injection of GSK923295 (125 mg/kg; B). (Scale bar: 50  $\mu$ m.)

**Table S1. CENP-E inhibitors**

Identifiers		GSK923295 (CAS #1088965–37-0)	GSK-1	GSK-2 (CAS #869567–90-8)
Structure				
IC50 (nM)	MT-stimulated*	2.3 $\pm$ 0.1	550 $\pm$ 106	3.7 $\pm$ 0.1
	basal <sup>†</sup>	2,078.0 $\pm$ 40	ND	7,367.0 $\pm$ 234
Steady-state mechanism of action	ATP	Uncompetitive $K_i$ app = 3.2 $\pm$ 0.2	competitive-like $K_i$ app = 4400 $\pm$ 132; $\alpha$ = 8 $\pm$ 0.3	uncompetitive-like $K_i$ app = 4.2 $\pm$ 0.3; $\alpha$ = 0.25 $\pm$ 0.04
	MT	Uncompetitive $K_i$ app = 3.1 $\pm$ 0.2	NA	uncompetitive $K_i$ app = 4.7 $\pm$ 0.2

All values determined with  $n = 4$  and displayed  $\pm$  SD. Units are nM.

\*IC50 determined at 5  $\times$  Km, ATP and 5  $\times$  Km, MT.

<sup>†</sup>IC50 determined at 5  $\times$  Km, ATP.

**Table S2. Kinetic constants for GSK923295 action on CENP-E motor domain**

CENP-E kinetic constants		No inhibitor (control)	+GSK923295
ATP-promoted MT dissociation*	$k_{max}$	$23 \pm 0.6 \text{ s}^{-1}$	
	$K_{1/2}$ , ATP	$59 \pm 4 \text{ }\mu\text{M}$	
	$k_{off}$ , MT	$0.14 \pm 0.002 \text{ }\mu\text{M s}^{-1\dagger}$	$8 \pm 0.1 \times 10^{-4} \text{ }\mu\text{M s}^{-1\dagger}$
mantATP binding	$k_{on}$	$0.9 \pm 0.08 \text{ }\mu\text{M s}^{-1}$	$1.27 \pm 0.15 \text{ }\mu\text{M s}^{-1}$
	$k_{off}$	$19.7 \pm 3.8 \text{ s}^{-1}$	$9.6 \pm 0.9 \text{ s}^{-1}$
Phosphate release <sup>‡</sup>	$k_{max}$	$7.2 \pm 0.1 \text{ s}^{-1}$	$39 \pm 0.7 \text{ s}^{-1}$
	$K_{1/2}$ , ATP	$44 \pm 6 \text{ }\mu\text{M}$	$11.8 \pm 0.8 \text{ }\mu\text{M}$
	$k_{off}$ , Pi	$0.044 \pm 0.001 \text{ }\mu\text{M s}^{-1\dagger}$	$2 \pm 0.7 \times 10^{-4} \text{ }\mu\text{M s}^{-1\dagger}$
mantADP release (with MTs) <sup>§</sup>	$k_{max}$	$63 \pm 4 \text{ s}^{-1}$	
	$K_{1/2}$ , MT	$4.8 \pm 1 \text{ }\mu\text{M}$	$0.009 \pm 0.004 \text{ }\mu\text{M s}^{-1¶}$
	$k_{off}$ , mantADP	$3.8 \pm 0.5 \text{ }\mu\text{M s}^{-1¶}$	
Inhibitor dissociation <sup>^</sup>	$t_{1/2}$	NA	10.2 hr
	$k_{off}$		0.068 hr <sup>-1</sup>

Presteady-state measurements were determined ( $n = 2$ ); steady-state measurements ( $n = 4$ ). Values are shown  $\pm$  SD.

\*Determined using turbidity.

<sup>†</sup>Fitted to a linear equation between 0 and 125  $\mu\text{M}$  ATP.

<sup>‡</sup>Determined using the fluorescent phosphate reporter N-(2-[1-maleimidyl]ethyl)-7-diethylamine-coumarin-3-carboxamide-phosphate binding protein (MDCC-PBP).

<sup>§</sup>Determined by competing mantADP with excess unlabeled MgATP.

<sup>¶</sup>Fitted to a linear equation between 0 and 16  $\mu\text{M}$  MTs.

<sup>^</sup>Determined by equilibrium dialysis.

**Table S3. Sensitivity to GSK923295 and functional characteristics of human, dog, and mouse CENP-E motor domains and mutants of human CENP-E**

Enzyme	Mutation	GSK923295 Ki (nM)	GSK-1 Ki (nM)	kcat ( $\text{s}^{-1}$ )	MT Km ( $\mu\text{M}$ )	ATP Km ( $\mu\text{M}$ )	Basal ATPase ( $\text{s}^{-1}$ )
Human	wt	$3.2 \pm 0.2$	$4.2 \pm 0.3$	$10.2 \pm 0.7$	$0.34 \pm 0.01$	$32 \pm 2$	$0.059 \pm 0.002$
Dog	wt	$1.6 \pm 0.1$	$2.4 \pm 0.2$	$11.1 \pm 0.5$	$0.38 \pm 0.04$	$34 \pm 2$	$0.32 \pm 0.003$
Mouse	wt	$67 \pm 5$	$89 \pm 9$	$10.1 \pm 0.4$	$0.55 \pm 0.02$	$25 \pm 2$	$0.31 \pm 0.005$
Human	I182L T183A K184T	$64 \pm 7$	$73 \pm 6$	$17.1 \pm 0.2$	$1.00 \pm 0.08$	$27 \pm 2$	$0.14 \pm 0.004$
Human	I182L	$14 \pm 2$	ND	$9.9 \pm 0.3$	$0.45 \pm 0.02$	$38 \pm 1$	$0.12 \pm 0.004$
Human	T183A	$13 \pm 2$	ND	$12.2 \pm 0.2$	$0.55 \pm 0.02$	$34 \pm 2$	$0.05 \pm 0.001$
Human	K184T	$12 \pm 3$	ND	$9.8 \pm 0.5$	$1.38 \pm 0.09$	$23 \pm 1$	$0.07 \pm 0.001$
Human	I182L T183A	$61 \pm 8$	ND	$12.4 \pm 0.2$	$0.46 \pm 0.01$	$42 \pm 2$	$0.08 \pm 0.001$
Human	I182L K184T	$18 \pm 4$	ND	$10 \pm 0.5$	$1.49 \pm 0.11$	$25 \pm 2$	$0.09 \pm 0.001$
Human	T183A K184T	$11 \pm 2$	ND	$12.1 \pm 0.2$	$1.81 \pm 0.14$	$20 \pm 1$	$0.06 \pm 0.001$

Measurements were determined ( $n = 4$ ). Values are shown  $\pm$  SD.

**Table S4. Antitumor activity of GSK923295 in xenograft models of human cancer**

Tumor cell line	Origin	Dose (mg/kg)	N	Endpoint (mm <sup>3</sup> )	T-C (days)	% TGD	PR	CR
Colo205	colon	125	5	1,000	>74	NA	4	1
		62.5	5	1,000	24.9	122	0	0
HT29	colon	125	5	1,000	18	39	0	0
		62.5	5	1,000	2.7	6	0	0
HCT116	colon	125	5	1,000	10.4	37	0	0
		62.5	5	1,000	-2.8	NA	0	0
A549	lung	125	10	900	25.3	73	7	0
		62.5	10	900	3.7	11	1	0
H460	lung	125	10	1,500	37.2	210	3	2
		62.5	10	1,500	15.4	87	2	1
H1299	lung	125	10	1,200	16.8	76	0	1
		62.5	10	1,200	3.3	15	0	2
MV522	lung	125	5	1,000	26.3	104	1	1
		62.5	5	1,000	12.5	50	0	0
MX1	breast	125	5	1,000	6.9	26	0	0
		62.5	5	1,000	1.4	5	0	0
MCF7	breast	125	9	1,000	15.8	58	0	1
		62.5	9	1,000	5.4	20	0	1
MDA-MB-231	breast	125	5	1,000	47.1	99	4	0
SKOV3	ovary	125	5	1,000	>95	NA	4	1
		62.5	5	1,000	71.6	194	1	1

T-C, difference between median time to endpoint (days) of treated versus control group; % TGD,  $[(T-C)/C] \times 100$ ; PR, partial regression; CR, complete regression; NA, not applicable.



**Movie S1.** HCC1954 cells engineered to stably express a GFP fusion of Histone 2B were cultured in a 96-well plate in medium supplemented with propidium iodide (PI) at 0.2  $\mu\text{g}/\text{mL}$ , and fluorescence images were acquired of GFP (white) and PI channels (red) every 15 min for 5 days.

[Movie S1](#)

## Other Supporting Information Files

**Dataset S1.** Sensitivity of tumor cell lines to GSK923295

[Dataset S1 \(XLS\)](#)